Sensors and Actuators A 265 (2017) 161–167

Contents lists available at ScienceDirect

Sensors and Actuators A: Physical

journal homepage: www.elsevier.com/locate/sna

Liquid refractometric sensors based on optical fiber resonators

M. Eryürek[a], Y. Karadag[b], M. Ghafoor[a,1], N. Bavili[a], K. Cicek[c,a], A. Kiraz[a,d,*]

[a] Department of Physics, Koç University, Rumelifeneri Yolu, 34450 Sarıyer, İstanbul, Turkey
[b] İstiklal Street, Birlik Avenue, No: 23, Ümraniye, İstanbul, Turkey
[c] Department of Electrical and Electronics Engineering, Iğdır University, Suveren Campus, 76000 Iğdır, Turkey
[d] Department of Electrical and Electronics Engineering, Koç University, Rumelifeneri Yolu, 34450 Sarıyer, İstanbul, Turkey

ARTICLE INFO

Article history:
Received 2 February 2017
Received in revised form 26 July 2017
Accepted 7 August 2017
Available online 12 August 2017

Keywords:
Optical fiber resonator
WGM
Tapered fiber
Ethanol
Ethylene glycol
Optical sensor
Liquid refractometry

ABSTRACT

A robust, easy-to-fabricate, and sensitive liquid refractometric sensor utilizing optical fiber resonators (OFRs) obtained by simple stripping and cleaning of conventional optical fibers is presented. The sensing scheme is based on recording the spectral changes of the whispering gallery modes (WGMs) observed in the transmission spectrum of an OFR excited with a tunable laser coupled to the OFR through an independent tapered optical fiber. The demonstrated sensor device is tested and fully characterized with water solutions of ethanol and ethylene glycol (EG). Good agreements are obtained with theoretical predictions for both ethanol and EG cases when TE and TM polarized WGMs are considered. The limit of detection of the demonstrated sensor is determined to be between 2.7 and 4.7 $\times 10^{-5}$ refractive index unit (RIU) comparable to the state-of-the-art when precise temperature control of the sample chamber is missing.

1. Introduction

Optical ring resonators possess high quality optical resonances, i.e. whispering gallery modes (WGMs), that circulate near the interface between the dielectric medium of the ring and the outside medium. WGMs can have considerable evanescent field intensities in close proximity (up to several hundred nanometers) to the ring resonator surface. This yields optical ring resonators well-suited for sensing the refractive index (RI) of the surrounding bulk medium [1–5]. Up to date different resonator geometries such as Fabry–Pérot cavities [6], microspheres [7–9], microrings [10], and liquid core optofluidic ring resonators [11–13] have been used in such demonstrations of bulk RI sensing. Changes in the bulk RI down to the order of 10^{-7} refractive index unit (RIU) could be detected in the experiments using optofluidic ring resonators [11] and microspheres [7].

Standard optical fibers can form cylindrical ring resonators hosting WGMs that reside near the fiber rims and circulate in planes perpendicular to the fiber axis [14–16]. They are easy to prepare following simple fiber stripping and cleaning, they have analytically predictable WGM properties [17], and their WGMs can possess high quality factors (Q-factors) exceeding 10^6 [14]. Despite these favorable properties, up to now only one work [16] studied bulk RI sensing with standard optical fiber resonators (OFRs). In that work WGMs with relatively low Q-factors ($Q < 500$) were employed, measurements were reported only for pure surrounding fluids (air, water, and ethanol) without a concentration dependent analysis revealing the minimum detection limit, and comparison of the sensitivity with theoretical predictions was not included.

Here, we present and fully characterize bulk RI sensors using optical ring resonators based on standard optical fibers. We achieve coupling of light to an individual OFR using a tapered optical fiber placed in perpendicular geometry [16,18]. Light from a tunable laser source is coupled to the tapered fiber and WGMs are monitored by measuring the tapered fiber transmission as a function of the laser wavelength. We use ethanol/water and ethylene glycol (EG)/water mixtures as test liquids and demonstrate measurements of ethanol and EG concentrations with sensitivities of 37 and 67 pm/%, respectively. Measurements with both ethanol and EG are in good agreement with theoretical predictions. Such a sensor for precise measurement of ethanol concentration in a solution can be used for a wide range of applications in chemical engineering, biotechnology, medicine and food industry [19–22]. Precise determination of EG concentration in a solution is also important

* Corresponding author.
E-mail address: akiraz@ku.edu.tr (A. Kiraz).
[1] Present addresses: Institute of Photonics, University of Eastern Finland, 80100 Joensuu, Finland; ITMO University, 190000 Saint Petersburg, Russia.

http://dx.doi.org/10.1016/j.sna.2017.08.019
0924-4247/

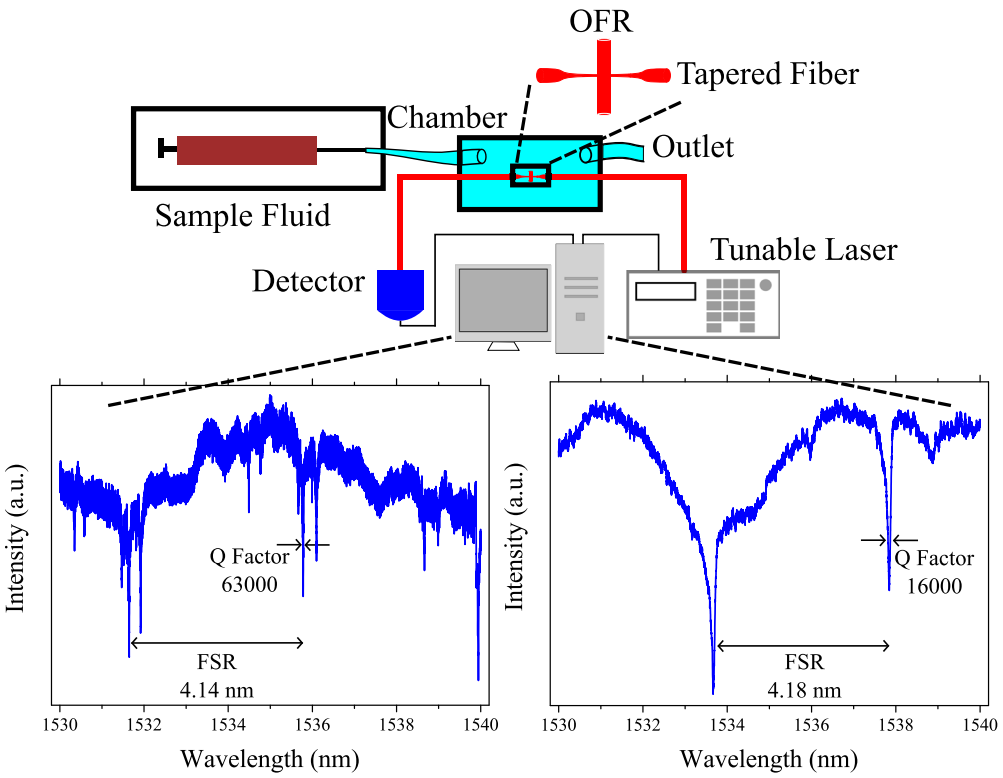

Fig. 1. (a) Schematic description of the fiber tapering and sensor characterization setups used in the experiments. Exemplary transmission spectra recorded from a sensor device while the chamber is filled with (b) air (*Q*-factor: 63000, FSR: 4.14 nm) and (c) water (*Q*-factor: 13000, FSR: 4.18 nm) are shown.

in applications including separation of ethanol/water mixtures [23] and synthesis of advanced materials [24].

2. Experimental

The experimental study is started with tapering of a standard single mode fiber (SMF). The polymeric layer of the SMF is removed mechanically and cleaned with isopropyl alcohol (IPA) and made ready for tapering. Fiber tapering is performed using a hydrogen flame while pulling the SMF from both ends utilizing computer-controlled motorized stages. Hydrogen flow rate is kept constant at 95 ml/min for the generation of the hydrogen flame. Following fiber pulling, the diameter of the tapered region becomes as thin as around 3.2 μm (see the inset in Fig. 1) which is sufficient for coupling light out from the tapered fiber. For avoiding the sagging of the tapered region of the fiber, the motorized stages moved further without the hydrogen flame. The additional pulling distance is chosen to be between 0.02 and 0.10 mm to ensure that the tapered region is straight.

Following fiber tapering, another standard SMF is stripped from the polymeric layer and cleaned with IPA, and then placed on the tapered fiber in a perpendicular position with respect to tapered region to serve as the OFR (Fig. 1(a)). Both the tapered fiber and the OFR are fixed with an epoxy glue to a printed circuit board, and wavelength dependent transmission of the tapered fiber was measured using a tunable laser (Santec, TSL-510-C, tuning range: 1500–1630 nm, wavelength resolution: 1 pm). The transmission spectrum of such an exemplary sensor when surrounded by air is shown in Fig. 1(b). The observed spectrum reveals a free spectral range (FSR) of 4.14 nm together with a Q-factor of 63000. Using Eqs. (1) and (2) with $n_{out} = 1$, $R = 62.5$ μm, and $\lambda \approx 1535$ nm, FSR value is found to be 4.15 nm (TM) or 4.16 nm (TE) for $n_{in} = 1.46$. This best fit value to the RI of the OFR is in agreement with the RI of typical glass materials at $\lambda \sim 1535$ nm [25].

Prepared sensor devices are then transferred to a sample chamber which allows for liquid flow. Fig. 1(c) shows the transmission spectrum obtained from a sensor device at this stage, when surrounded by water. From this spectrum, the *Q*-factor of the resonance modes decreases to 16,000 mainly due to water absorption and the presence of contaminants in the liquid. FSR observed in Figs. 1(b) and (c) are 4.14 and 4.18 nm, in good agreement with the predictions from Eqs. (1) and (2) which reveal FSR = 4.15–4.16 nm (TM and TE) for $n_{in} = 1.46$, $n_{out} = 1$ or $n_{out} = 1.3183$, $R = 62.5$ μm, and $\lambda \approx 1535$ nm.

The picture of the sample chamber is provided in Fig. 2. In the beginning of each experiment, deionized (DI) water is injected into the chamber using a syringe pump to make sure that the solute concentration is 0%. Then ethanol/water or EG/water solution is introduced into the chamber at a required concentration using the syringe pump. During the experiments tapered fiber transmission spectra are continuously recorded. Spectral shifts of individual WGMs are determined by post-processing using a Gaussian curve fitting algorithm [26].

3. Spectral positions of the WGMs

Spectral positions of the WGMs have been analytically calculated for the OFR geometry used in the experiments. The calculation involves solving the Helmholtz equation and applying boundary conditions for an infinitely-long cylinder. For TM and TE excitations, the coefficients of the field amplitudes are respectively given by [17]

$$a_l = \frac{J_l'(y)J_l(x) - mJ_l(y)J_l'(x)}{J_l'(y)H_l(x) - mJ_l(y)H_l'(x)} \quad (1)$$

$$b_l = \frac{mJ_l'(y)J_l(x) - J_l(y)J_l'(x)}{mJ_l'(y)H_l(x) - J_l(y)H_l'(x)} \quad (2)$$

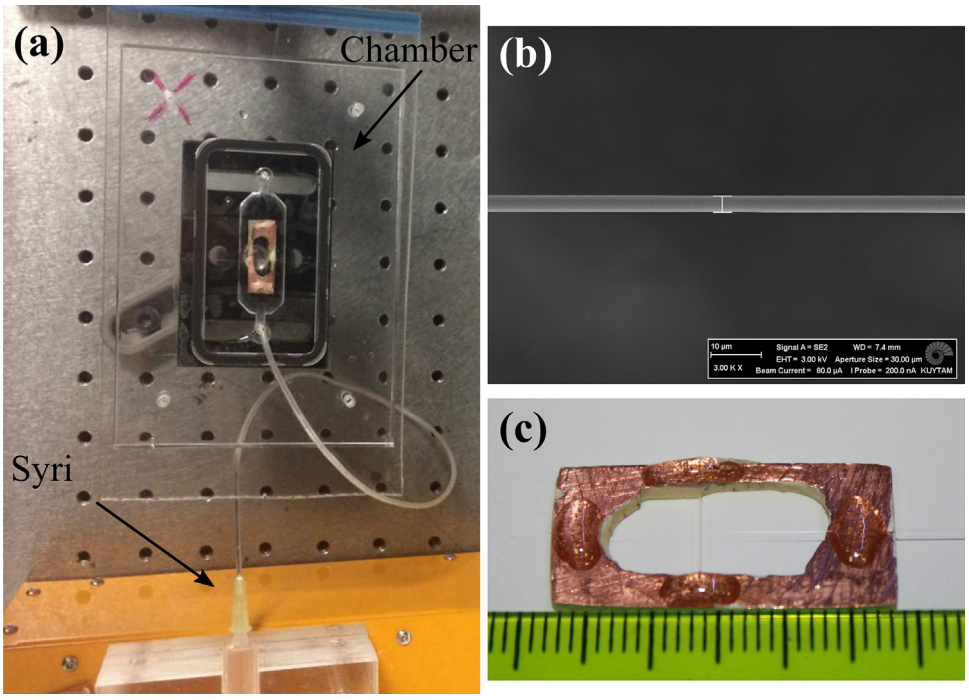

Fig. 2. (a) Picture of the sample chamber with the detector and the syringe pump. (b) An SEM image of a tapered fiber. Scale bar is 10 μm. The thickness at the thinnest portion of the tapered fiber is measured to be ~3.2 μm. (c) Holder for the OFR and tapered fiber. Scale increases by 1 mm.

where J_l is the lth-order Bessel function of the first kind, H_l is the lth-order Hankel function of the first kind and m is the relative RI between the inside and outside of the resonator, i.e. $m = n_{in}/n_{out}$. The arguments of the functions J_l and H_l are defined as $x = 2\pi R n_{out}/\lambda$, also known as the size parameter, and $y = m\ x$. R, λ and l represent the radius of the resonator, wavelength of the light in vacuum and azimuthal mode number, respectively. If the electric (magnetic) field of the excitation is parallel to the cylindrical symmetry axis of the OFR, WGMs are defined to have TE (TM) polarization, according to the convention from the reference [17]. WGMs are observed for size parameters when the denominators of a_l and b_l become equal to zero. Results of the theoretical calculations showing the spectral shift values ($\Delta\lambda$) of the first radial order WGMs for different ethanol or EG volume/volume concentrations (c_{ETH} or c_{EG}) in water ($n_w = 1.3183$ at $\lambda = 1535$ nm [25]) are shown in Fig. 3. In these calculations the RI of the OFR is taken to be $n_{OFR} = 1.46$ based on the best fit to the free spectral range (FSR) observed in the transmission spectrum shown in Fig. 1(b), assuming $R = 62.5$ μm. $\Delta\lambda$ values are calculated for specific first radial order WGMs which have $l = 362$ with starting resonant wavelengths of 1537.68 nm (TE) and 1536.17 nm (TM) when the ambient medium is pure water. The RI of the pure water ambient medium is changed with c_{ETH} or c_{EG} based on the references [27,28]. In [27,28], RI of ethanol/water and EG/water solutions with different concentrations are provided assuming $\lambda = 589$ nm at 20 °C. We convert these RI values to $\lambda = 1535$ nm, assuming the changes in RI with concentration of the substance follow similar trends as in Ref. [27,28] except for normalization factors that are obtained by comparing RI values of pure water, ethanol and EG at $\lambda = 589$ nm with those values at $\lambda = 1535$ nm [25]. RI values of pure ethanol and EG are considered to be 1.3506 and 1.4199, respectively at $\lambda = 1535$ nm [25]. Total RI of the ambient medium (n_{amb}) as a function of ethanol or EG concentration is depicted in the inset in Fig. 3. Using these values for n_{OFR} and n_{amb}, expected $\Delta\lambda$ values are calculated as a function of c_{ETH} or c_{EG} with Eqs. (1) and (2) for both TM and TE polarizations. The resulting sensitivities to bulk RI changes and solute concentration are listed in Table 1. For small concentration changes around

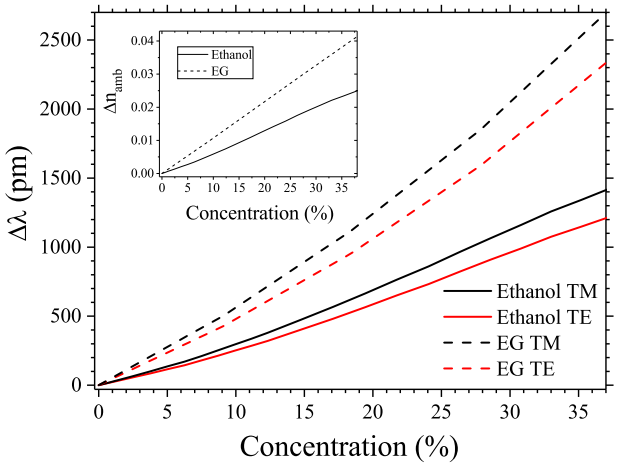

Fig. 3. Calculated spectral shift values ($\Delta\lambda$) of the WGMs with respect to ethanol and EG concentrations. First radial order WGMs are considered which have $l = 362$ with starting resonant wavelengths of 1537.68 nm (TE) and 1536.17 nm (TM) when the ambient medium is pure water. EG calculation yields a higher slope since EG has a higher RI contrast with water than the RI contrast of ethanol with water. Inset shows the assumed change in the RI of the solutions as a function of the ethanol or EG concentration.

Table 1
Calculated bulk RI sensitivity and concentration sensitivity values for the OFR.

Solute	Conc.	Bulk RI sens. [nm/RIU]		Conc. sens. [pm/%]	
		TM	TE	TM	TE
Ethanol	0%	62.9	55.3	25.7	22.6
EG	0%	62.6	56.8	50.8	46.1
Ethanol	35%	90.9	78.1	39.9	34.3
EG	35%	114.1	100.6	88.0	77.6

0%, bulk RI sensitivities of $\Delta\lambda$ are obtained as ~63 nm/RIU and ~55–56 nm/RIU for TM and TE cases, independent of the solute added to water. For concentration changes around 35%, sensitiv-

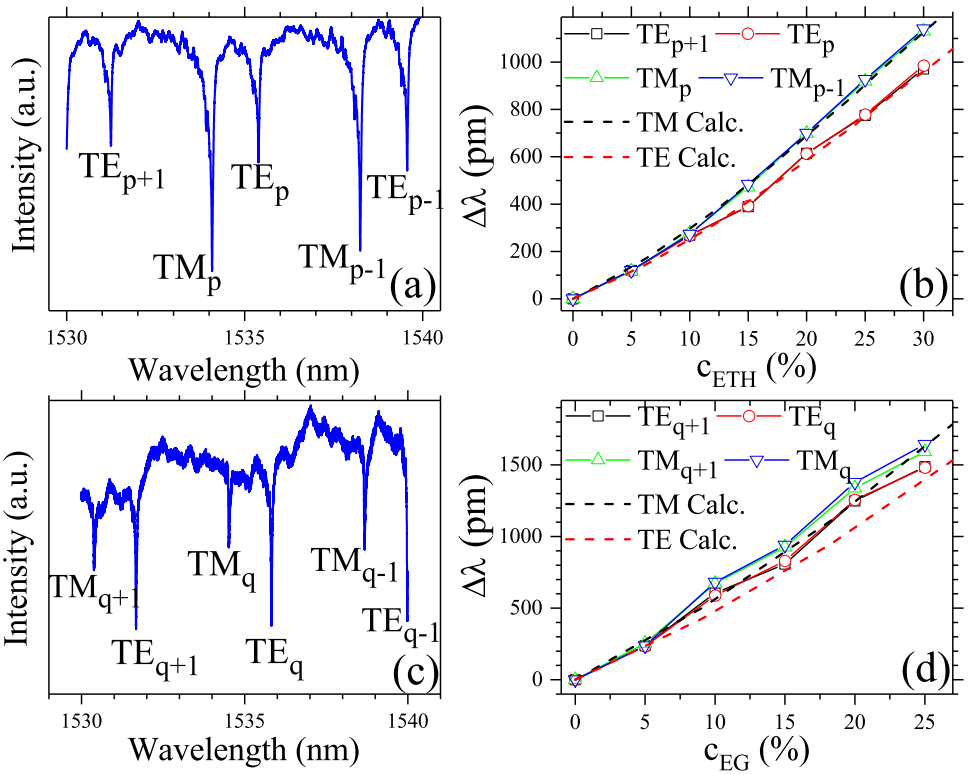

Fig. 4. Exemplary transmission spectra recorded during experiments using water solutions of (a) ethanol and (c) EG. From the WGMs depicted in the transmission spectra, four were selected for analysis under changing concentrations of ethanol or EG. Respective spectral shifts of the WGMs are depicted in (b) and (d) together with the theoretical predictions for TE and TM polarizations shown by dashed lines.

ities become equal to 90.9 nm/RIU (TM) and 78.1 nm/RIU (TE) for ethanol, and 114.1 nm/RIU (TM) and 100.6 nm/RIU (TE) for EG. On the other hand, sensitivities of $\Delta\lambda$ to concentration are obtained as 25.7 pm/% (TM, ethanol), 22.6 pm/% (TE, ethanol), 50.8 pm/% (TM, EG) and 46.1 pm/% (TE, EG) for concentration changes around 0%, and 39.9 pm/% (TM, ethanol), 34.3 pm/% (TE, ethanol), 88.0 pm/% (TM, EG) and 77.6 pm/% (TE, EG) for concentration changes around 35%.

4. Results

In Fig. 4 we show the results of sensing experiments performed for both ethanol and EG cases where two different mode families (TE and TM) are visible in the transmission spectra together with theoretical predictions. In each of these cases the spectral positions of four WGMs which are depicted in Figs. 4(a) and (c) are tracked while the bulk RI was changed. Subscripts denote the azimuthal mode numbers for the corresponding WGMs. Despite the fact that both Figs. 4(a) and (c) show the transmission spectra recorded when the ambient liquid is water, in these figures WGMs with the same azimuthal mode number and polarization appear at slightly different spectral positions. This is mainly attributed to slight deviation of the angle between the tapered fiber and the OFR from 90°. Each data point in Figs. 4(b) and (d) indicates the spectral shift observed in a specific WGM after sufficient waiting time (~10 min) following the injection of the bulk liquid at a certain concentration. Modes denoted with TM (TE) indicate the WGMs which are more (less) sensitive to bulk RI changes, in agreement with theoretical predictions shown by dashed curves in Fig. 4. The difference between the measured spectral shift values for TM and TE cases is between 9–22% for concentrations larger than 10%, in agreement with the calculated values of 16–18%. Very good agreements are observed between the experimental and calculated concentration sensitivities for both ethanol and EG cases shown in Fig. 4(b) (experimental sensitivities of 39 pm/% (TM) and 33 pm/% (TE) as compared to the calculated sensitivities of 38.1 pm/% (TM) and 32.6 pm/% (TE) in the concentration range 0–30%) and Fig. 4(d) (experimental sensitivities of 67 pm/% (TM) and 61 pm/% (TE) as compared to the calculated sensitivities of 60.4 pm/% (TM) and 51.8 pm/% (TE) in the concentration range 0–25%).

Sensitivity curves and exemplary spectral shift time traces recorded in other ethanol and EG sensing experiments employing one of the WGMs observed in the transmission spectra are shown in Fig. 5. In these experiments, after the sample liquid is exchanged with a different concentration solution, saturation levels are reached in a few minutes without fluctuations except for the cases when multiple syringe shots are injected after one another. The resonance shift closely follows the changes in concentration. Response of the OFR begins to increase just after a couple of minutes and exponentially reaches the saturation level. At each plateau of concentration after the saturation is reached, 10 data points are averaged and $\Delta\lambda$ values are calculated. These values are then plotted and depicted in Figs. 5(b) and (d).

Our experimental setup does not allow for direct detection of the polarization of the WGMs. Instead of a direct measurement, polarizations of the WGMs are determined by analysis of multiple transmission spectra. We consider the transmission spectra where both TE and TM mode families are observed. In such cases, among the two WGMs with the same mode number, TM polarization is assigned to the one with smaller wavelength. This mode identification procedure is further supported by the sensitivities of the WGMs to RI changes. We always observed the TM WGMs to be slightly more sensitive to RI changes than TE WGMs, in agreement with the theoretical predictions shown in Fig. 4. From the data presented in Fig. 5 average concentration sensitivities are obtained as 34 (TE, ethanol), 39 (TM, ethanol), 63 (TE, EG), and 71 pm/% (TM, EG)

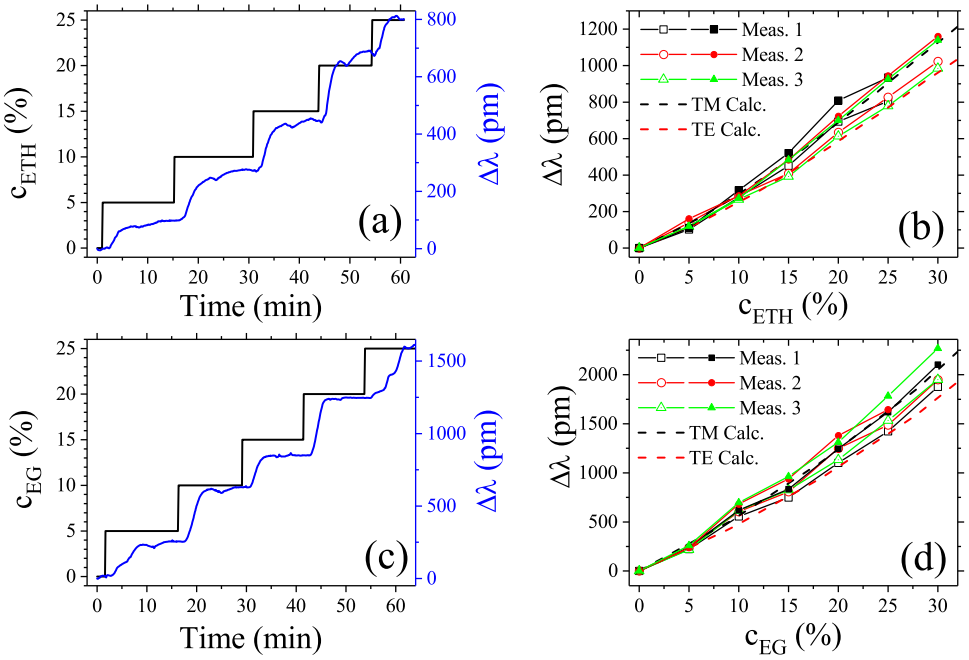

Fig. 5. Exemplary time traces of Δλ values observed in (a) ethanol and (c) EG measurements. Changes in Δλ values follow changes in the concentration very closely. In (b) and (d), results from multiple measurements are plotted for ethanol and EG, respectively. For each measurement, spectral traces of multiple WGMs are shown with the same color. Depending on the polarization of the examined mode, the indicated symbols are either full or void for TM and TE polarizations, respectively.

for ethanol and EG concentrations between 0–30%. For both ethanol and EG, the average experimental concentration sensitivity values are very close to theoretical predictions which reveal sensitivities of 32.1 (TE, ethanol), 37.7 (TM, ethanol), 53.8 (TE, EG), and 62.5 pm/% (TM, EG) for a concentration range of 0–30% (Figs. 5(b) and (d)).

In order to characterize the reversibility of the sensors, hysteresis experiments are performed where ethanol or EG concentration is gradually increased from 0% to 20% and then decreased back to 0%. Exemplary spectral shift time traces and sensitivity curves obtained from three such hysteresis experiments for ethanol and EG are shown in Fig. 6. In these experiments the polarizations of the WGMs are indirectly determined, as discussed for Fig. 5. For a certain concentration, hysteresis is mathematically defined as the difference between $\Delta\lambda_{forw}$ and $\Delta\lambda_{back}$, normalized to $\Delta\lambda_{forw}$, where $\Delta\lambda_{forw}$ and $\Delta\lambda_{back}$ are amounts of shifts during increasing and decreas-

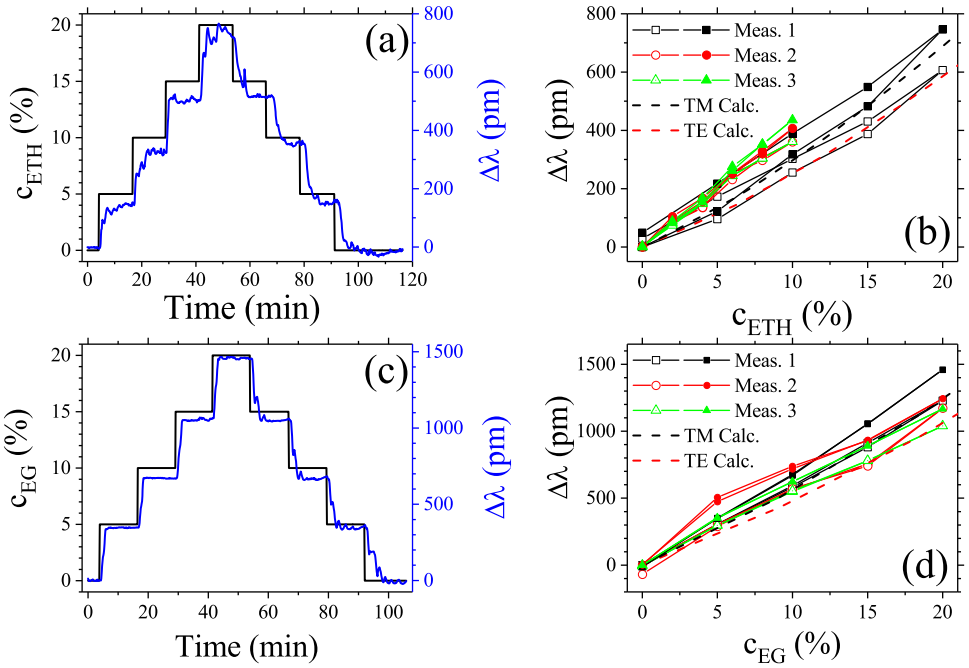

Fig. 6. Exemplary time traces of Δλ values observed during hysteresis experiments performed with (a) ethanol and (c) EG. Changes in Δλ values follow changes in the concentration very closely. In (b) and (d), results from multiple measurements are plotted for ethanol and EG, respectively. For each measurement, spectral traces of multiple WGMs are shown with the same color. Depending on the polarization of the examined mode, the indicated symbols are either full or void for TM and TE polarizations, respectively.

ing concentrations. Average hysteresis values calculated from Figs. 6(b) and (d) are 15% (TE, ethanol), and 17% (TM, ethanol), 2% (TE, EG), and 1% (TM, EG). In both of these figures, analytical calculations are plotted together with the experimental results. Average sensitivities deduced from Fig. 6 for ethanol and EG are 34 (TE, ethanol), 40 (TM, ethanol), 56 (TE, EG), and 63 pm % (TM, EG). Similar to Figs. 4 and 5, sensitivity values observed for both ethanol and EG are in good agreement with theoretical predictions which reveal sensitivities of 29.1 (TE, ethanol), 34.1 (TM, ethanol), 48.0 (TE, EG), and 56.3 pm/% (TM, EG) for a concentration range of 0–20% (Figs. 6(b) and (d)).

In order to determine the limit of detection (LOD) of our liquid refractometric sensor, we calculate the standard deviation of the measurements performed with a constant solute concentration. The uncertainty in spectral shift measurements is determined from the standard deviation of data points as 2.6 pm in Fig. 6(a) between $t = 59.56–68.68$ min (75 data points), and 1.7 pm in Fig. 6(c) between $t = 6.75–16.65$ min (80 data points). Based on Table 1, these minimum detectable spectral shifts correspond to LOD values of 4.7×10^{-5} (TE, ethanol), 4.1×10^{-5} (TM, ethanol), 3.0×10^{-5} (TE, EG), and 2.7×10^{-5} (TM, EG) RIU. The observed LOD values can be further improved by implementing a better thermal control to the sample chamber [11].

5. Conclusion

A liquid refractometric optical sensor utilizing OFRs obtained from standard SMFs is studied both theoretically and experimentally. Sensing mechanism relies on spectral shifts of WGMs excited in the azimuthal direction of the OFR using a tapered fiber. The reliability of the sensor is verified with experiments using ethanol/water and EG/water solutions. WGMs with different polarizations are observed to show slightly different sensitivities when the solute concentration is changed. Average sensitivities to solute concentrations are measured to be 34 (39) and 63 (71) pm/% for ethanol and EG cases for TE (TM) polarization for a concentration range of 0–30%, in good agreement with theoretical predictions. LOD of the demonstrated sensor is shown to be between 2.7 and 4.7×10^{-5} RIU. The observed LOD can be further improved by implementing a closed loop thermal control of the sample chamber. Hence, the presented robust, easy-to-fabricate, and sensitive optical refractometric sensor constitutes an attractive alternative to other optical refractometric sensor technologies.

Acknowledgments

We acknowledge financial support from TÜBİTAK (Grant Nos. 110T803 and 115F446) and thank Alexandr Jonáš for proofreading the manuscript.

References

[1] I.M. White, H. Oveys, X. Fan, Liquid-core optical ring-resonator sensors, Opt. Lett. 31 (2006) 1319–1321.
[2] X. Fan, I.M. White, S.I. Shopova, H. Zhu, J.D. Suter, Y. Sun, Sensitive optical biosensors for unlabeled targets: a review, Anal. Chim. Acta 620 (1–2) (2008) 8–26.
[3] Y. Sun, X. Fan, Optical ring resonators for biochemical and chemical sensing, Anal. Bioanal. Chem. 399 (1) (2011) 205–211.
[4] Y. Zhi, X.-C. Yu, Q. Gong, L. Yang, Y.-F. Xiao, Single nanoparticle detection using optical microcavities, Adv. Mater. 29 (2017) 1604920.
[5] B.-B. Li, W.R. Clements, X. Yu, K. Shi, Q. Gong, Y.-F. Xiao, Single nanoparticle detection using split-mode microcavity Raman lasers, Proc. Natl. Acad. Sci. U. S. A. 111 (2014) 14657–14662.
[6] R. St-Gleais, J. Masson, Y.-A. Peter, All-silicon integrated Fabry–Pérot cavity for volume refractive index measurement in microfluidic systems, Laser Photon. Rev. 8 (2014) 521–547.
[7] N.M. Hanumegowda, C.J. Stica, B.C. Patel, I. White, X. Fan, Refractometric sensors based on microsphere resonators, Appl. Phys. Lett. 87 (20) (2005).
[8] T. Ioppolo, N. Das, M.V. Ötügen, Whispering gallery modes of microspheres in the presence of a changing surrounding medium: a new ray-tracing analysis and sensor experiment, J. Appl. Phys. 107 (10) (2010).
[9] Y. Zhi, T. Thiessen, A. Meldrum, Single quantum dot coated microspheres for microfluidic refractive index sensing, J. Opt. Soc. Am. B 30 (2012) 51–56.
[10] U. Levy, K. Campbell, A. Groisman, S. Mookherjea, Y. Fainman, On-chip microfluidic tuning of an optical microring resonator, Appl. Phys. Lett. 88 (11) (2006).
[11] H. Li, X. Fan, Characterization of sensing capability of optofluidic ring resonator biosensors, Appl. Phys. Lett. 97 (1) (2010).
[12] M. Sumetsky, R.S. Windeler, Y. Dulashko, X. Fan, Optical liquid ring resonator sensor, Opt. Express 15 (2007) 14376–14381.
[13] J. Wang, T. Zhan, G. Huang, P.K. Chu, Y. Mei, Optical microcavities with tubular geometry: properties and applications, Laser Photon. Rev. 8 (2014) 521–547.
[14] H.-J. Moon, Y.-T. Chough, K. An, Cylindrical microcavity laser based on the evanescent-wave-coupled gain, Phys. Rev. Lett. 85 (2000) 3161–3164.
[15] Q. Chen, M. Ritt, S. Sivaramakrishnan, Y. Sun, X. Fan, Optofluidic lasers with a single molecular layer of gain, Lab Chip 14 (2014) 4590–4595.
[16] A. Boleininger, T. Lake, S. Hami, C. Vallance, Whispering gallery modes in standard optical fibres for fibre profiling measurements and sensing of unlabelled chemical species, Sensors 10 (3) (2010) 1765.
[17] H.C. Van de Hulst, Light Scattering by Small Particles, 2nd ed., Dover Publications Inc., 1981.
[18] J. Villatoro, D. Monzon-Hernandez, E. Mejia, Fabrication and modeling of uniform-waist single-mode tapered optical fiber sensors, Appl. Opt. 42 (2003) 2278–2283.
[19] S. Alpat, A. Telefoncu, Development of an alcohol dehydrogenase biosensor for ethanol determination with toluidine blue o covalently attached to a cellulose acetate modified electrode, Sensors 10 (2010) 748–764.
[20] Y. Sun, B.Y. Shekunov, P. York, Refractive index of supercritical CO_2–ethanol solvents, Chem. Eng. Commun. 190 (1) (2003) 1–14.
[21] M. Mukhopadhyay, B.S. Rao, Modelling of supercritical drying of ethanol-soaked silica aerogels with carbon dioxide, J. Chem. Technol. Biotechnol. 83 (2008) 1101–1109.
[22] B. Hahn-Hägerdal, M. Galbe, M.F. Gorwa-Grauslund, G. Liden, G. Zacchi, Bio-ethanol – the fuel of tomorrow from the residues of today, Trends Biotechnol. 24 (2006) 549–556.
[23] E. Quijada-Maldonado, G.W. Meindersma, A.B. de Haan, Viscosity and density data for the ternary system water (1)-ethanol(2)-ethylene glycol(3) between 298, 15 K and 328.15 K, J. Chem. Thermodyn. 57 (2013) 500–505.
[24] M.-G. Ma, Y.-J. Zhu, J.-F. Zhu, Z.-L. Xu, A simple route to synthesis of $BaCO_3$ nanostructures in water/ethylene glycol mixed solvents, Mater. Lett. 61 (2007) 5133–5136.
[25] M.N. Polyanskiy, Refractive index database, Available at: http://refractiveindex.info (accessed December 2016).
[26] M. Eryürek, Y. Karadag, N. Tasaltin, N. Kilinc, A. Kiraz, Optical sensor for hydrogen gas based on a palladium-coated polymer microresonator, Sens. Actuators B 212 (2015) 78–83.
[27] D.R. Lide, CRC Handbook of Chemistry and Physics, Internet Version 2005, CRC Press, 2005 hbcponline.com.
[28] E.T. Fogg, A.N. Hixson, A.R. Thompson, Densities and refractive indexes for ethylene glycol–water solutions, Anal. Chem. 27 (1955) 1609–1611.

Biographies

M. Eryürek was born in Razgrad, Bulgaria in 1987. He received his B.Sc. degree from Bilkent University, Physics Department in 2010 and his M.Sc. degree from Koç University, Optoelectronics and Photonics Engineering Program in 2013. He is currently pursuing his Ph.D. in Koç University, Physics Department.

Y. Karadag received his B.Sc. (2007) in physics from Bilkent University. He received his M.Sc. (2009) and Ph.D. degrees (2013) in physics from Koç University. In 2013, he joined TUBITAK BILGEM as a senior researcher where he worked on development of high power lasers. He has been an assistant professor at Marmara University, Physics Department between 2014 and 2016. His research interests are optofluidics and tapered fiber spectroscopy.

M. Ghafoor was born in Pakistan in 1994. He received his BS in Engineering Sciences from GIK Institute in 2015. He is currently working on his thesis for his double masters degree in Photonics and Advanced Materials and Technologies in Photonics from University of Eastern Finland and ITMO University respectively. He joined the Optofluidics and Nanooptics research group at Koç University as an intern in the summers of 2016 and worked on this project.

N. Bavili was born in Tabriz, Iran in 1989. He received his B.Sc. degree from Tabriz University, Physics Department in 2012 and his M.Sc. degree from Istanbul Technical University (ITU), Physics Engineering Program in 2015. He joined Koç University Optofluidics and Nano-Optics Research Laboratory in July 2016 to pursue his Ph.D. education.

K. Cicek received his PhD in Electrical and Electronic Engineering from University of Bristol, UK in 2016. Currently he is an assistant professor in the department of Electrical and Electronic Engineering in Igdir University, Turkey. He also holds the position of research collaborator at University of Bristol. His Research interests are photonic and optoelectronic devices and their applications.

A. Kiraz is a professor in the physics and electrical-electronics engineering departments at Koç University. He received his B.S. degree in electrical-electronics engineering from Bilkent University in 1998, M.S. and Ph.D. degrees in electrical and computer engineering from the University of California, Santa Barbara in 2000 and 2002, respectively. Between 2002 and 2004 he worked as a post-doctoral associate at the Institute for Physical Chemistry in the Ludwig-Maximilians University, Munich, and received Alexander von Humboldt fellowship. He joined Koç University in 2004 and became a full professor in 2014. Between 2014 and 2015 he was a visiting professor at the Biomedical Engineering of the University of Michigan, Ann Arbor. His current research interests include optofluidics, single molecule spectroscopy/microscopy, optical manipulation, and biomedical instrumentation. His research team pursues various research projects targeting the development of novel micro-optical devices, optofluidic lab-on-a-chip devices, molecular and gas sensors, optofluidic-based renewable energy solutions, and confocal microscope device concepts. He is a member of SPIE and senior member of OSA.